Sustainable Energy, Grids and Networks 31 (2022) 100736

Contents lists available at ScienceDirect

Sustainable Energy, Grids and Networks

journal homepage: www.elsevier.com/locate/segan

# Green ammonia production-enabled demand flexibility in agricultural community microgrids with distributed renewables

Lawryn Edmonds [a], Peter Pfromm [b], Vincent Amanor-Boadu [c], Mary Hill [d], Hongyu Wu [a,*]

[a] Mike Wiegers Department of Electrical and Computer Engineering, Kansas State University, 1701D Platt Street Manhattan, KS, USA
[b] The Gene and Linda Voiland School of Chemical Engineering and Bioengineering, Washington State University, 1505 Stadium Way Pullman, WA, USA
[c] Department of Agricultural Economics, Kansas State University, 1603 Old Claflin Place Manhattan, KS, USA
[d] Department of Geology, University of Kansas, 1414 Naismith Drive Lawrence, KS, USA

ARTICLE INFO

*Article history:*
Received 11 November 2021
Received in revised form 18 February 2022
Accepted 24 April 2022
Available online 5 May 2022

*Keywords:*
Renewable energy
Distribution locational marginal price
Green ammonia
Fuel cell
Agricultural microgrid

ABSTRACT

Currently, manufactured ammonia relies on natural gas or coal, which releases harmful carbon emissions. We investigate the viability of a small-scale "green" ammonia plant where renewable electricity is used to provide hydrogen via electrolysis and nitrogen via air liquefaction to a Haber–Bosch system to synthesize ammonia. The relatively small scale, and measures such as continuous preheating, are envisioned to provide response times on the order of minutes rather than the days required by prevalent large-scale, fossil fuel-based ammonia plants. A green ammonia plant can serve as a demand-responsive load and long-term energy storage mechanism (through chemical energy storage in ammonia). We investigate its functional and economic viability within an agricultural community microgrid, which is a new contribution to this area of study. This paper proposes a coordinated operational mixed-integer linear programming (MILP) model of an electricity distribution system and an electricity-run, green ammonia plant enabled by the Haber–Bosch process. Case studies in both grid-connected and islanded modes are performed on an agricultural community microgrid based on a modified Pacific Gas & Electric (PG&E) 69-node electricity distribution system coupled with a flexible, small-scale ammonia plant and direct ammonia fuel cell. Results indicate the ammonia plant can adequately serve as a demand response resource and positively impact the distribution locational marginal price (DLMP) by reducing or removing voltage violations and line congestion in the system. Studies showed this coupling decreased electricity costs of the ammonia plant by nearly a third, with ammonia profits increasing 17%. Further, in an emergency, the direct ammonia fuel cell can provide essential power. This cooperation among the food–energy–water (FEW) network offers a unique solution to the challenge of a more efficient interconnection of renewable energy (RE) resources to the grid. Additionally, this work has the potential to reduce grid dependence on fossil fuels and aid in the decarbonization of ammonia production.

© 2022 Elsevier Ltd. All rights reserved.

## 1. Introduction

Modern power distribution systems have seen an increase in renewable energy (RE) technologies in recent years. With characteristics of variability and uncertainty, these resources pose challenges for the aging power grid that was not originally engineered to operate in this manner [1]. Mismatched power load and generation has always been problematic. One of the significant operational challenges of RE penetration is the mismatch that occurs due to the uncertain and variable generation output from RE sources along with the increasing unpredictability of customer demands due to an increased penetration of distributed energy resources (DERs), such as small-scale wind and rooftop photovoltaic (PV) technologies. Imbalances can lead to load shedding, curtailed power generation, or the operation of base load generators when it is not economical or necessary [2]. Solutions proposed in the literature for this challenge typically include an increase of energy storage resources and or demand response techniques [3]. If excess renewable energy generation is present in the system, energy can be stored and used later, so it does not go to waste. On the other hand, if there is insufficient generation in the system to match the load, flexible loads allow the energy demand to follow the potentially fast-changing (on the order of minutes/hours) generation supply. Further, authors in [4] indicate sufficient operating reserve, through energy storage, demand response, and flexible generators, reduces the cost of integrating variable renewables into power grids.

* Corresponding author.
*E-mail address:* hongyuwu@ksu.edu (H. Wu).

https://doi.org/10.1016/j.segan.2022.100736
2352-4677/© 2022 Elsevier Ltd. All rights reserved.

Storage options typically include traditional battery energy storage, thermal energy storage [5], and pumped hydro storage [6,7]. These storage options, particularly conventional battery energy storage, face degradation of energy capacity over charging and discharging cycles, short storage times, and thermal runaway. Therefore, long-term (more than one day) energy storage solutions should be explored. Ammonia can be consumed by a direct ammonia fuel cell to provide energy to the grid in times of need, which can serve as another method to address the variability of renewable energy resources. Therefore, cooperation between electricity distribution systems and green ammonia plants offers a unique solution to grid integration of renewable resources.

We propose a framework for a rural agricultural community microgrid to alleviate the aforementioned challenges. Community microgrids benefit both the community and the grid and have characteristics of (1) spanning a large area and benefitting many customers, (2) can be owned by a utility, and (3) lowering system costs by deploying DERs at optimal locations. In contrast, traditional microgrids are owned by individual customers and typically only benefit that single customer or a few surrounding customers and do very little for the grid [8]. The cooperation between a rural energy system and an ammonia synthesis plant reduces peak electricity loads and allows chemical energy storage in the form of ammonia to mitigate renewable generation curtailment. Utility operators can shift ammonia plant electricity demands to best serve the utility so long as the desired amount of ammonia is produced by the end of a given time frame. In return, the ammonia plant must be rewarded for providing these services to the electrical system.

Buying and selling energy at the true cost of electricity at a node is one method to accurately reward active resources in the distribution grid. A technique that achieves this is the distribution location marginal price (DLMP) mechanism, which is the marginal cost to serve the next unit of power at a node. This method is similar to the locational marginal price (LMP) mechanism used in the electric transmission market today. With characteristics of fair, transparent, and cost-causation prices, this mechanism is very desirable for future distribution markets integrating various distributed energy resources [9]. A financial incentive for ancillary services to ease operational issues such as voltage violations and congestion on lines comes from the integration of this mechanism, as DLMPs are higher when these issues arise in the system.

Ammonia is the focus of this work largely due to its importance to agriculture. Bio-available nitrogen is essential for all life and is central to the food–energy–water (FEW) nexus. Manufactured, nitrogen-rich ammonia ($NH_3$) and derivatives like urea are used to fertilize crops. The use of ammonia fertilizers is responsible for about 40% of the global food production today [10,11]. It has been proven that ammonia used as fertilizer can substantially increase crop yields for the same input of water [10]. Many farmers use the anhydrous ammonia produced by the plant considered in this work for crop fertilizer, and ammonia production consumes 30%–50% of the energy used for crop production [10]. Consequently, an ammonia plant serving as a flexible demand to the distribution grid can provide a commodity that can be used locally. Further, the global transport of ammonia is well established. Existing infrastructure allows for bulk ammonia to be transported by pipeline, road, rail, and ship [12]. Finally, the use of ammonia as an energy vector (for hydrogen) is receiving considerable attention [13–16], suggesting the existence of a viable market for energy stored as ammonia.

Most large-scale ammonia producers do not rely on substantial amounts of electricity for ammonia synthesis today. Typically, natural gas or coal is used as the fuel and or hydrogen source for ammonia production, and $NH_3$ is condensed using the century-old Haber–Bosch process. This procedure is referred to as "brown" ammonia. However, in the procedure studied in this work, the ammonia is produced by deriving hydrogen ($H_2$) from water, through the energy-intensive water electrolysis procedure, along with sourcing nitrogen ($N_2$) through an air separation unit. The $N_2$ and $H_2$, called syngas, are then fed into the existing Haber–Bosch catalyst to create $NH_3$. If the electricity used to power this process is generated from renewable resources, the output is referred to as "green" ammonia. Fig. 1 outlines the procedure for ammonia synthesis considered in this work. This procedure decarbonizes ammonia production. Ammonia produced using fossil fuels produces an estimated 670 million metric tons of fossil carbon dioxide ($CO_2$) emissions per year [17]. Green ammonia used as fertilizer can help lower the dependence of food on fossil fuels while aiding in the decarbonization of ammonia production.

Electricity-run green ammonia plants are not a new concept, with the first research published in this area in the 1960s. Pioneering work published in 1977 proposes the concept of storing wind energy in the form of hydrogen [18], but the process has only recently approached economic feasibility. With the increase in low-cost renewable energy technologies being added to the grid, electricity prices have decreased in recent years [19], making more environmentally friendly ammonia production feasible. Yet, the economics for synthesizing brown ammonia still slightly outperform the method proposed in this paper. With the energy demand of green ammonia and brown (natural gas) ammonia being 7.7 $MWh/ton_{NH_3}$ [20] and 32.75 $MBTU/ton_{NH_3}$ (9.6 $MWh/ton_{NH_3}$) [21], and at the ten year (2010–2019) annual average cost of natural gas at \$3.3021/MBTU [22], electricity prices will have to drop from current levels of about \$0.1353/kWh in the U.S. in 2020 [23] to below \$0.014/kWh for the traditional method of synthesizing ammonia using natural gas to be less economical. The economics for green ammonia improve with penalties/taxes for releasing carbon monoxide and carbon dioxide into the atmosphere or incentives/premiums for green products. Independently, the price of electricity is expected to fall in the coming years. This price of electricity may be achievable within 10–15 years as renewable generation and battery storage increase. Less reliance on traditional power plants, which have comparatively higher operation and maintenance costs, will also contribute to a decline in the price of electricity. These trends favor lower electricity prices and greater economic competitiveness of green ammonia.

Using the true cost of electricity through the DLMP mechanism can also be beneficial to green ammonia. There may be times of very low DLMP values throughout the day, and the ammonia plant can take advantage of this by consuming electricity during these times.

Further, the start-up and shut-down of green ammonia synthesis plants involve the three main sections of the process: hydrogen production via electrolysis, nitrogen production via membrane-based or cryogenic air separation, and ammonia synthesis via the Haber–Bosch synthesis loop. The main challenge for rapid start-up is heating the Haber–Bosch reactor to around 200–300 °C. This can be avoided by preheating the reactor at all times, which requires negligible energy (relative to the total energy required to synthesize ammonia) for a reactor with sufficient heat management. Further, membrane-based nitrogen production (with subsequent polishing to remove trace oxygen) and electrolysis [24] are comparatively flexible operations. Therefore, green ammonia plants have excellent potential to serve as demand-responsive loads to the electricity grid.

To illustrate the rapid changes taking place, consider that the energy demand of green ammonia has recently reduced from around 10.4 $MWh/ton_{NH_3}$ to 7.7 $MWh/ton_{NH_3}$ (the value used

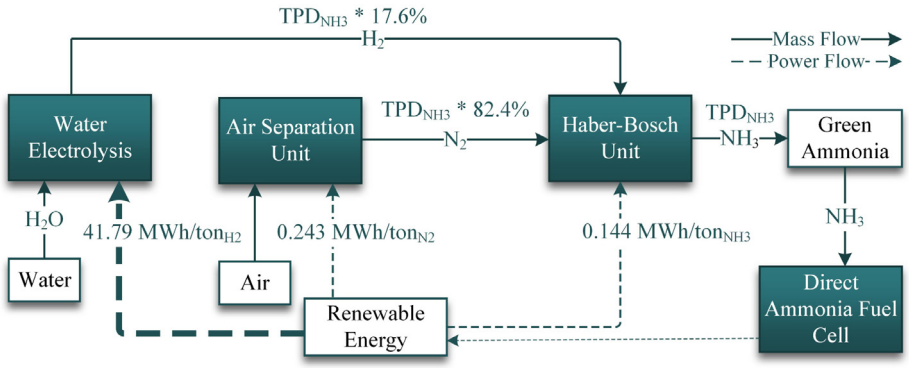


**Fig. 1.** Proposed green ammonia plant procedure. Arrow width indicates relative size of energy transfer. Power consumption rates provided here are discussed in Section 3. (TPD = tons per day).

above) due to a breakthrough in the commercialization of a solid oxide electrolysis cell in the water electrolysis procedure [20].

In part because of the rapid changes, the energy management of green ammonia plants has not been well researched to this date, to the best of the authors' knowledge. Further, the impact of energy flexibility from green ammonia plants and direct ammonia fuel cells on the DLMP is yet to be explored.

There are many tangentially related papers within the realm of electrification of ammonia production. A recent, comprehensive review of the production, distribution, and storage of nitrogen-based alternative fuels, including green ammonia, is provided in [25]. Further, authors in [12,26] provide reviews of ammonia applications for power as well as the many factors that arise therefrom. This area gained significant attention in the late 2010s with substantial work that investigates electrolytic hydrogen synthesis [27], green ammonia synthesis/power-to-ammonia (P2A) [28–33], and power-to-ammonia-to-power (P2A2P) technology [34]. Authors in [35] provide a process analysis of renewable-powered ammonia production, focusing on solar power. However, these works mainly focus on the feasibility of these processes rather than the coupling between the ammonia and electricity sectors.

More specifically, many distantly related papers consider the planning of these two systems. For example, an alternating direction method of multipliers algorithm is used in [36] to solve a co-planning model to optimize wind generation and ammonia plant(s) siting and configuration as well as electricity transmission system expansion with respect to total investment and operational costs. While this work considers power balance constraints and direct current (DC) power flow modeling, real-time or day-ahead scheduling of the two systems is beyond the scope of this work. Additionally, authors in [37] consider joint planning of hydrogen production and electrical systems to enable high levels of variable renewable energy resources and energy system decarbonization. This work also analyzes the marginal cost of electricity under different hydrogen demand scenarios.

Further, under a similar concept to the research proposed in this paper, our previous work [38] considers flexibility and energy storage in drinking water pumps and elevated water tanks, respectively, when optimizing a day-ahead schedule in a distribution system. Authors in [39] consider flexibility within an integrated natural gas and electricity transmission system, including hydrogen production via electrolysis and steam methane reforming. A day-ahead scheduling model considering transmission grid and gas network constraints is provided. Authors in [40] consider hydrogen (from electrolysis) production flexibility in transmission grids with variable renewable energy sources and consider DC power flow and balance constraints. Additionally, [41,42] consider electrolytic hydrogen synthesis while considering transmission grid constraints, while [42] considers locational electricity pricing. It is important to consider this transmission-level interaction, but the models cited above do not focus on distribution systems, especially future distribution systems with diverse distributed energy resources.

Complementary to this research, authors in [43] propose a multi-energy (electrical, ammonia, and thermal energy carriers) thermo-electrochemical model with thermal and power balancing constraints. Still, physical grid constraints were not considered. The proposed methodology was tested on a laboratory-level, small-scale microgrid. A comparison of various storage techniques, including P2A, traditional battery storage, and power-to-gas (P2G) applications, such as rapid response electrolysis for methane ($CH_4$) and hydrogen ($H_2$) is described. Authors in [44] evaluate the thermodynamic performance and energy efficiency of solar-powered intermittency mitigation by way of clean ammonia synthesis and direct ammonia fuel cells. The formulation developed in [45] is used to optimally schedule wind-powered ammonia generation with respect to least-cost annual operations. Authors in [46] provide a combined capacity planning and scheduling of green ammonia production. Though the aforementioned works consider ammonia as a storage medium for excess renewable generation and power balance constraints, they do not consider physical grid constraints. Therefore, the impact of this procedure on the grid and the DLMP appears to be a fruitful area of inquiry.

The novelty of the work presented here resides in the quantitative consideration of a combined electricity distribution system and ammonia production plant with constraints in a day-ahead or real-time scheduling problem. The impact of the coordination of the ammonia plant on the DLMP will be explored to discover the optimal operation of an electricity distribution system and an ammonia plant.

For the first time, we investigate the viability of a green ammonia production plant to serve as a demand-responsive load to the electric power system and test this concept on a realistic electricity distribution system. To achieve this, we propose a mixed-integer linear programming (MILP) model of a merged power system and ammonia plant to optimally schedule DERs, electricity loads, and ammonia production, which is the first model of this kind. Here, the flexible electricity demand from the ammonia production is coupled with the total electricity demand. Power-to-ammonia-to-power applications are also considered using a direct ammonia fuel cell to provide power to the electricity grid. When the demand is greater than the generation in the power system or when the price of producing electricity is high, the ammonia plant responds to this price by reducing its electricity load to aid in the power balancing of the electric grid. When there is excess RE generation in the local system,

the plant produces and stores more ammonia. The excess ammonia is stored in tanks and sold into the ammonia market or even fed back into the power system through direct ammonia fuel cells. This P2A2P process using a fuel cell has a round-trip efficiency of around 30% [47]. This procedure is only favorable in islanded or emergency situations due to the costliness of consuming ammonia which could otherwise sell for higher profits in the bulk ammonia market. Further, the present-day power output of commercial fuel cells is still relatively small, typically in kilowatts.

The coupling proposed in this paper can reduce electricity costs and renewable energy curtailment. When there is insufficient ramping down capability in thermal units or power line congestion, RE curtailment typically occurs, reducing the utilization of available wind and PV energy [48]. The proposed electricity model does not consist of thermal units with ramping constraints; therefore, RE curtailment is caused by congested lines and voltage violations. This model is optimized from the perspective of the distribution system operator (DSO) and considers physical constraints of both the ammonia plant and the electricity distribution system. The electricity costs of powering the green ammonia plant determine a significant portion of the operational costs and control the economics to make this process competitive with brown ammonia plants. Therefore, ammonia plant operational costs are reduced when the cost of supplying electricity is minimized.

A community microgrid based on a modified Pacific Gas & Electric (PG&E) 69-node electricity distribution system is coupled with a demand-responsive ammonia plant is used to perform case studies. Under the future case of a distribution market (as described in [49]), the capability of anhydrous ammonia to serve as a storage medium of excess renewable energy is examined. Supplying energy using marginal operating costs is a central focus of future distribution markets. Thus, the impact on the DLMP from the cooperation of the green ammonia plant is studied. The contributions of this work are as follows:

(1) A novel MILP model for coordinated operation of an electricity distribution system and ammonia plant while considering DLMP in the model is proposed. Constraints for a small-scale, green ammonia plant are modeled for the first time in this work.
(2) For the first time, the effect of the ammonia plant and electrical system coordination in a future distribution market considering a high penetration of renewable energy and DLMPs is shown. The capability of the ammonia plant in reducing line congestion and voltage violations in the electricity distribution system is examined.
(3) To investigate the resiliency of an agricultural community microgrid, an emergency case is considered. We examine a case where wind turbines are shut down for safety purposes, and only critical loads are met. The impact of a direct ammonia fuel cell serving the community in times of need is explored.

The remainder of this paper is organized as follows. We outline the mathematical model for the electricity distribution system and ammonia plant and fuel cell in Sections 2 and 3, respectively. Case studies utilizing anhydrous ammonia as a storage medium for excess RE and its impact on the DLMP are provided in Section 4. We provide important observations and conclude the work in Section 5.

## 2. Electricity distribution model

An unbalanced three-phase electricity distribution system or agricultural community microgrid is considered. Modified DistFlow equations with losses are used. This model is adapted from our previous work in [50]. We index the substation node or the point of common coupling (PCC) as 0 and order the rest of the nodes from 1 to $\mathcal{N}$, where $\mathcal{N}$ is the total number of nodes/lines. As shown in Fig. 2, line $i$ is the line connecting the upstream node, $u(i)$, and the set of downstream nodes, $d\{i\}$, to node $i$. All variables related to line $i$ are subscripted by index $i \in \mathcal{N}$, for phase $\phi \in \Phi$, and time $t \in \mathcal{T}$.

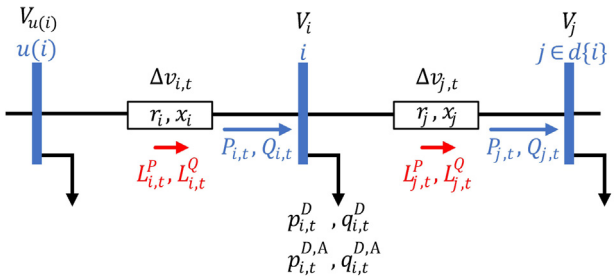


**Fig. 2.** Distribution branch with line $i$ connecting bus $u(i)$ to node $i$. The total electrical load is comprised of non-ammonia base loads ($p^D_{i,t}$) and ammonia plant ($p^{D,A}_{i,t}$) demands. Here, $r_i$ and $x_i$ are line resistance and reactance.

### 2.1. Objective function

The objective function, defined in (1), is the least cost sum of operating the electrical distribution system and is captured in $C^E$.

$$C^E = \sum_{\phi,t} \lambda^{p_0}_t \cdot p_{0,\phi,t} + \sum_{\phi,t} \lambda^{q_0}_t \cdot q_{0,\phi,t} + \sum_{i,\phi,t} c^{G,P}_{i,\phi,t} \cdot p^G_{i,\phi,t} + \sum_{i,\phi,t} c^{G,Q}_{i,\phi,t} \cdot q^G_{i,\phi,t} + \sum_{i,\phi,t} \xi^R \cdot s^R_{i,\phi,t} \quad (1)$$

The real and reactive LMP prices at the substation node connected to the transmission system are represented by $\lambda^{p_0}_t$ and $\lambda^{q_0}_t$, and the real and reactive net power injections at the substation node are $p_{0,\phi,t}$ and $q_{0,\phi,t}$, which is assumed to be an infinite source. Negative net power injections indicate the DSO is buying real or reactive power from the distribution system at the LMP of the substation node. Distributed generators (DGs) bid at $c^{G,P}_{i,\phi,t}$ for real power and $c^{G,Q}_{i,\phi,t}$ for reactive power. Here, the marginal cost of the generator is used as the bid of the DG. The real and reactive power supplied by the generators are indicated by $p^G_{i,\phi,t}$ and $q^G_{i,\phi,t}$. The reactive power output of the DG must lie within a fraction, $\kappa^G$, of the real power output. The RE resources bid at \$0/MWh and are therefore not present in the objective function. Similarly, under the assumption these assets are owned by the DSO, the battery energy storage system (BESS) units and the direct ammonia fuel cell do not bid into the market. Instead, these resources operate to best serve the needs of the system. The final term in (1) penalizes RE curtailment ($s^R_{i,\phi,t}$) at a value of $\xi^R$. This is to discourage inefficient utilization of the RE resources in the system. Note the RE generation is curtailed equally across all phases.

### 2.2. Power balance

Constrains (2)–(3) model the total system real and reactive power balance. Here $L^P_{i,\phi,t}$ and $L^Q_{i,\phi,t}$ are the linearized real and reactive power losses. The real and reactive power net node injection ($p_{i,\phi,t}$, $q_{i,\phi,t}$) are modeled in (4)–(5). Variables $p^D_{i,\phi,t}$ and $q^D_{i,\phi,t}$ are the real and reactive system power demands and $p^R_{i,\phi,t}$ and $q^R_{i,\phi,t}$ are the real and reactive RE unit outputs. Real and reactive BESS outputs are represented by $p^B_{i,\phi,t}$ and $q^B_{i,\phi,t}$, and the

real and reactive direct ammonia fuel cell outputs are represented by $p^{FC}_{i,\phi,t}$ and $q^{FC}_{i,\phi,t}$. Reactive fuel cell generation is restricted to $\kappa^{FC}$ of the dispatched real fuel cell generation.

$$p_{0,\phi,t} + \sum_{i}(p_{i,\phi,t} + L^{P}_{i,\phi,t}) = 0 \tag{2}$$

$$q_{0,\phi,t} + \sum_{i}(q_{i,\phi,t} + L^{Q}_{i,\phi,t}) = 0 \tag{3}$$

$$p_{i,\phi,t} = p^{D}_{i,\phi,t} - p^{G}_{i,\phi,t} - p^{B}_{i,\phi,t} - p^{R}_{i,\phi,t} - p^{FC}_{i,\phi,t} \tag{4}$$

$$q_{i,\phi,t} = q^{D}_{i,\phi,t} - q^{G}_{i,\phi,t} - q^{B}_{i,\phi,t} - q^{R}_{i,\phi,t} - q^{FC}_{i,\phi,t} \tag{5}$$

$$p^{B}_{i,\phi,t} = \hat{p}^{B}_{i,\phi,t} - \check{p}^{B}_{i,\phi,t} \tag{6}$$

$$p^{R}_{i,\phi,t} = \overline{p}^{R}_{i,\phi,t} - s^{R}_{i,\phi,t} \tag{7}$$

$$0 \le s^{R}_{i,\phi,t} \le \overline{p}^{R}_{i,\phi,t} \tag{8}$$

The net real power extraction of the BESS ($p^{B}_{i,\phi,t}$), defined in (6), is the difference between the extraction ($\hat{p}^{B}_{i,\phi,t}$) and injection ($\check{p}^{B}_{i,\phi,t}$) power. The reactive power of the battery, $q^{B}_{i,\phi,t}$, must lie within zero and $\kappa^{B}$ of the real power BESS extraction. Constraints defining the state of charge, dis/charging rates, and the minimum number of dis/charging hours of the BESS can be found in our previous work [51].

Eq. (7) determines the dispatched real RE generation, $p^{R}_{i,\phi,t}$, from the expected generation, $\overline{p}^{R}_{i,\phi,t}$. Penalized in the objective function, the difference is captured in $s^{R}_{i,\phi,t}$. The positive curtailment is limited to a value less than the expected generation (8). Reactive RE generation is held within $\kappa^{R}$ of the dispatched real RE generation.

### 2.3. Distribution power flow

Defined in (9) and (10), the real and reactive power flows are represented by variables $P_{i,\phi,t}$ and $Q_{i,\phi,t}$. Nodal voltage, $v_{i,\phi,t}$, is defined in (11) in reference to the substation voltage, $v_{0,\phi,t}$. System parameters $\mathcal{M}^{P}_{i,\phi,j}$ and $\mathcal{M}^{Q}_{i,\phi,j}$ are comprised of upstream and downstream incidence matrices and line resistance and reactance diagonal matrices [52]. Originally quadratic relations of the real and reactive power flow, line impedance, and nodal voltage, real and reactive power losses ($L^{P}_{i,\phi,t}$, $L^{Q}_{i,\phi,t}$) are approximated using a first-order Taylor series approximation around an exogenously obtained feasible point [53]. Specifics on the approximated loss is presented in our previous work [52]. Voltage and line limit bounds are enforced by constraints (12) and (13), respectively. Here, $\epsilon$ is a small value, normally 5%, and $\overline{S}_{i,\phi}$ is the maximum MVA line limit. The initially convex quadratic apparent power flow limit, $|P_{i,\phi,t}|^2 + |Q_{i,\phi,t}|^2 \le \overline{S}^2_{i,\phi}$, is linearly approximated in (13). Obtained from *Convex Optimization of Power Systems* [54], this equation models the outer approximation of the system power flow. The real and reactive power imbalance between phases at the substation node are restricted by (14) and (15) within a small percentage, $\Delta\phi_p$ and $\Delta\phi_q$, respectively.

$$P_{i,\phi,t} = p_{i,\phi,t} + \sum_{k\in d\{i\}}(p_{k,\phi,t} + L^{P}_{k,\phi,t}) \tag{9}$$

$$Q_{i,\phi,t} = q_{i,\phi,t} + \sum_{k\in d\{i\}}(q_{k,\phi,t} + L^{Q}_{k,\phi,t}) \tag{10}$$

$$v_{i,\phi,t} = v_{0,\phi,t} - \sum_{k\in\mathcal{N}} \mathcal{M}^{P}_{i,\phi,k} \cdot (p_{k,\phi,t} + L^{P}_{k,\phi,t}) - \sum_{k\in\mathcal{N}} \mathcal{M}^{Q}_{i,\phi,k} \cdot (q_{k,\phi,t} + L^{Q}_{k,\phi,t}) \tag{11}$$

$$1 - \epsilon \le v_{i,\phi,t} \le 1 + \epsilon \tag{12}$$

$$|P_{i,\phi,t}| + |Q_{i,\phi,t}| \le \sqrt{2}\cdot \overline{S}_{i,\phi} \tag{13}$$

$$|p_{i,\phi,t} - p_{i,\phi',t}| = \Delta\phi_p \quad \forall\phi \in \Phi, \forall\phi' \in \{\Phi\backslash\phi\} \tag{14}$$

$$|q_{i,\phi,t} - q_{i,\phi',t}| = \Delta\phi_q \quad \forall\phi \in \Phi, \forall\phi' \in \{\Phi\backslash\phi\} \tag{15}$$

An unbalanced, three-phase, real and reactive distribution system optimization model is represented in (1)–(13) and accounts for DGs, RE units, BESSs, fuel cells, and green ammonia plant loads. Validated in our previous work using commercially available electricity model software (MATPOWER), the accuracy of the electricity distribution model measurements can be verified in Ref. [52].

### 2.4. DLMP decomposition

Our linearized DLMP model, decomposed in Ref. [52], is leveraged here and extended to include the flexible demand of the green ammonia plant. The DLMP components remain the same for this case as the ammonia plant demand and fuel cell generation are not directly related to a marginal increase in electricity demand. Shown in (16)–(17), energy, loss, voltage violation, and congestion components are summed to the total real and reactive DLMP ($\Omega^{P}_{i,\phi,t}$, $\Omega^{Q}_{i,\phi,t}$).

$$\Omega^{P}_{i,\phi,t} = \Omega^{E_P}_{\phi,t} + \Omega^{L_P}_{i,\phi,t} + \Omega^{V_P}_{i,\phi,t} + \Omega^{C_P}_{i,\phi,t} \tag{16}$$

$$\Omega^{Q}_{i,\phi,t} = \Omega^{E_Q}_{\phi,t} + \Omega^{L_Q}_{i,\phi,t} + \Omega^{V_Q}_{i,\phi,t} + \Omega^{C_Q}_{i,\phi,t} \tag{17}$$

$$\Omega^{L_P}_{i,\phi,t} = \Omega^{E_P}_{\phi,t} \sum_{j\in\mathcal{N}} \frac{\partial L^{P}_{j,\phi,t}}{\partial p_{i,\phi,t}} + \Omega^{E_Q}_{\phi,t} \sum_{j\in\mathcal{N}} \frac{\partial L^{Q}_{j,\phi,t}}{\partial p_{i,\phi,t}} \tag{18}$$

$$\Omega^{L_Q}_{i,\phi,t} = \Omega^{E_Q}_{\phi,t} \sum_{j\in\mathcal{N}} \frac{\partial L^{Q}_{j,\phi,t}}{\partial q_{i,\phi,t}} + \Omega^{E_P}_{\phi,t} \sum_{j\in\mathcal{N}} \frac{\partial L^{P}_{j,\phi,t}}{\partial q_{i,\phi,t}} \tag{19}$$

$$\Omega^{V_P}_{i,\phi,t} = \sum_{i'}(v^{min}_{i',\phi,t} - v^{max}_{i',\phi,t}) \frac{\partial V_{i',\phi,t}}{\partial p_{i,\phi,t}} \tag{20}$$

$$\Omega^{V_Q}_{i,\phi,t} = \sum_{i'}(v^{min}_{i',\phi,t} - v^{max}_{i',\phi,t}) \frac{\partial V_{i',\phi,t}}{\partial q_{i,\phi,t}} \tag{21}$$

$$\Omega^{C_P}_{i,\phi,t} = \sum_{j\in u\{i\}} \rho^{1}_{i,\phi,t} \frac{\partial S_{j,\phi,t}}{\partial p_{i,\phi,t}} \tag{22}$$

$$\Omega^{C_Q}_{i,\phi,t} = \sum_{j\in u\{i\}} \rho^{2}_{i,\phi,t} \frac{\partial S_{j,\phi,t}}{\partial q_{i,\phi,t}} \tag{23}$$

The real and reactive energy components of the DLMP ($\Omega^{E_P}_{\phi,t}$, $\Omega^{E_Q}_{\phi,t}$) are determined by the shadow prices of (2) and (3). If the substation node is providing the next marginal unit of power, these values are equal to the LMP ($\lambda^{p_0}_{t}$, $\lambda^{q_0}_{t}$) at the substation node. Real and reactive loss components ($\Omega^{L_P}_{i,\phi,t}$, $\Omega^{L_Q}_{i,\phi,t}$) are determined by loss sensitivities with respect to nodal power injections. Similarly, voltage components ($\Omega^{V_P}_{i,\phi,t}$, $\Omega^{V_Q}_{i,\phi,t}$) are determined by voltage sensitivities to nodal power injections. The shadow prices of (12) on all nodes $i'$ that meet a lower or upper voltage limit are captured in $v^{min}_{i',\phi,t}$ and $v^{max}_{i',\phi,t}$. Finally, congestion components ($\Omega^{C_P}_{i,\phi,t}$, $\Omega^{C_Q}_{i,\phi,t}$) are determined by lines' apparent power flow sensitivities with respect to nodal power injections. The combinations of the four Lagrange multipliers that come from expanding the absolute values in (13) to a linear form are captured in $\rho^{1}_{i,\phi,t}$ and $\rho^{2}_{i,\phi,t}$. The combination of real and reactive power injections is captured in $S_{j,\phi,t}$ [52].

## 3. Ammonia plant and fuel cell model

Similar to the electrical system, indices $i \in \mathcal{N}$, $\phi \in \Phi$, $t \in \mathcal{T}$ are used. Here, $i$ is the node where the ammonia plant and fuel

cell connect to the electricity distribution system. We consider a balanced, three-phase, real and reactive load for the green ammonia plant. Through the use of advanced power electronics, the direct ammonia fuel cell is capable of providing real and reactive power to the system [55,56].

### 3.1. Ammonia plant model

The electricity demand and production tracking of an ammonia plant are modeled by constraints (24)–(39). The electrical load for ammonia ($p^{D,A}_{i,\phi,t}$) is comprised of hydrogen production from water electrolysis, nitrogen production from air separation, and ammonia condensation through the Haber–Bosch process. The chemical formula for ammonia production using this procedure is $6H_2O + 2N_2 \rightarrow 4NH_3 + 3O_2$. Hydrogen production requires, by far, the largest amount of energy to run. Assumed at a consumption of 41.79 $MWh/ton_{NH_3}$ of $H_2$, this process requires 17.6% of the tons of ammonia produced in $H_2$ [17]. The nitrogen production assumes a rate of 0.243 $MWh/ton_{NH_3}$ of $N_2$ while requiring 82.4% of the tons of ammonia produced in $N_2$ [17]. The Haber–Bosch process requires 0.144 $MWh/ton_{NH_3}$ of energy to operate. In total, and as defined in (24), the energy demand per metric ton ($MWh/ton_{NH_3}$) rate ($p^{D,AR}$) for this process is 7.7 $MWh/ton_{NH_3}$ [20].

The power demand of the ammonia plant depends on the operational mode of the plant and is captured in (24). We consider the load equivalent across all three phases of the distribution feeder; therefore, the total power demand is divided by three and equally assigned to each phase. To ensure the ammonia produced is categorized as "green" ammonia, the total demand must be less than the total renewable power in the system at a given time, $\sum_{i,\phi} p^{R}_{i,\phi,t}$, as in (25). Binary indicators $\mathbb{I}^{A}_{i,\phi,t}$ and $\mathbb{I}^{P}_{i,\phi,t}$ allow for 'on', 'off', and 'warming' modes. If the plant is 'on' ($\mathbb{I}^{A}_{i,\phi,t} = 1$) and producing ammonia ($\mathbb{I}^{P}_{i,\phi,t} = 1$), the power demand is a linear relationship between the production rate and the amount of ammonia produced in metric tons in that timeslot, $A^{P}_{i,t}$. To reduce the energy consumption when the price of electricity is high, a 'warming' mode is considered. The Haber–Bosch reactor can be warmed at a significantly lower power demand than when producing ammonia due to the high energy demand of water electrolysis. Considering maintaining British thermal units, a warming model allows for the minimization of shut-down and start-up operations. If the plant is 'on' ($\mathbb{I}^{A}_{i,\phi,t} = 1$), but not producing ammonia ($\mathbb{I}^{P}_{i,\phi,t} = 0$), it is in the 'warming' mode and the power demand is a constant based on the energy necessary for warming the reactor, $p^{D,W}$. Finally, if the plant is 'off' ($\mathbb{I}^{A}_{i,\phi,t} = 0$), which is a rare case but is included in this model for completeness, there is no power demand. Note, the plant is not allowed to be 'off' ($\mathbb{I}^{A}_{i,\phi,t} = 0$) and producing ammonia ($\mathbb{I}^{P}_{i,\phi,t} = 1$) at the same time, as enforced in (26). Note, the power demand for the 'off' mode is also reflected in (24) when $\mathbb{I}^{A}_{i,\phi,t}$ and $\mathbb{I}^{P}_{i,\phi,t}$ both equal '0' and there is no ammonia produced when $\mathbb{I}^{A}_{i,\phi,t}$ is '0', as enforced in (27).

We consider the ammonia plant a demand response system that produces $A^{P}_{i,t}$ tons of ammonia in an hour. The amount of ammonia produced in a timeslot must fall between the minimum ($\underline{A}^{P}$) and maximum ($\overline{A}^{P}$) amount of ammonia capable of being produced in that time frame (27). Note, if the plant is not producing ammonia, the amount produced in that timeslot is zero. At the end of the time frame ($\mathcal{T}$), the summed amount of ammonia produced in a timeslot ($A^{P}_{i,t}$) and the ammonia consumed by the fuel cell ($A^{FC}_{i,\phi,t}$), must sum to at least $\underline{A^{S}_{i}}$ metric tons per day (TPD), as determined by the ammonia plant owner (28). In the case of excess renewables and thus low-cost electricity, the ammonia plant can produce more ammonia to best benefit the utility in reducing voltage violations and line congestion. The excess renewable energy is stored in ammonia. It can then be used as fertilizer on-site, sold into the ammonia market, or consumed to produce electricity using a fuel cell.

The feedstock of ammonia ($A^{S}_{i,t}$), and the reduction due to its use by the fuel cell, is tracked as in (29), and must not exceed the maximum amount of ammonia capable of being stored on-site, $\overline{A^{S}_{i}}$. In the first timeslot, $A^{S}_{i,t-1}$ is the initial value of the feedstock of ammonia and is available for fuel cell use at the beginning of the day.

$$p^{D,A}_{i,\phi,t} = \frac{p^{D,W}}{3} \cdot (\mathbb{I}^{A}_{i,\phi,t} - \mathbb{I}^{P}_{i,\phi,t}) + \frac{p^{D,AR}}{3} \cdot A^{P}_{i,t} \tag{24}$$

$$\sum_{i,\phi} p^{D,A}_{i,\phi,t} \leq \sum_{i,\phi} p^{R}_{i,\phi,t} \tag{25}$$

$$\mathbb{I}^{P}_{i,\phi,t} \leq \mathbb{I}^{A}_{i,\phi,t} \tag{26}$$

$$\underline{A}^{P} \cdot \mathbb{I}^{P}_{i,\phi,t} \leq A^{P}_{i,t} \leq \overline{A}^{P} \cdot \mathbb{I}^{P}_{i,\phi,t} \tag{27}$$

$$A^{S}_{i,\mathcal{T}} \geq A^{S}_{i,0} + \underline{A^{S}_{i}} \tag{28}$$

$$A^{S}_{i,t} = A^{S}_{i,t-1} + A^{P}_{i,t} - \sum_{\phi} A^{FC}_{i,\phi,t} \leq \overline{A^{S}_{i}} \tag{29}$$

For best performance, we consider the ammonia plant to remain 'on' for a minimum of $UT_i$ number of hours and 'off' for a maximum of $DT_i$ hours. Eqs. (30) and (33) ensure the 'on' ($T^{on}_{i,\phi,t}$) and 'off' ($T^{off}_{i,\phi,t}$) time counters are positive and do not exceed the scheduling horizon limit ($\mathcal{T}$). Eqs. (31) and (34) increase the respective counter by one if the unit remains 'on' or 'off'. The minimum number of consecutive hours 'on' and the maximum number of consecutive hours 'off' are constrained by (32) and (35) with the use of binary 'on' and 'off' indicators, $\mathbb{I}^{on}_{i,\phi,t}$ and $\mathbb{I}^{off}_{i,\phi,t}$, which are '1' in the timeslot the plant turns 'on' or 'off', and '0' otherwise. These indicators must not both be activated in the same timeslot (36). If there is a change in the plant's 'on'/'off' status within two timeslots the respective indicator will capture this change (37).

$$0 \leq T^{on}_{i,\phi,t} \leq \mathcal{T} \cdot \mathbb{I}^{A}_{i,\phi,t} \tag{30}$$

$$(\mathcal{T}+1) \cdot \mathbb{I}^{A}_{i,\phi,t} - \mathcal{T} \leq T^{on}_{i,\phi,t} - T^{on}_{i,\phi,t-1} \leq 1 \tag{31}$$

$$T^{on}_{i,\phi,t} \geq UT_i \cdot \mathbb{I}^{off}_{i,\phi,t+1} \tag{32}$$

$$0 \leq T^{off}_{i,\phi,t} \leq \mathcal{T} \cdot (1 - \mathbb{I}^{A}_{i,\phi,t}) \tag{33}$$

$$1 - (\mathcal{T}+1) \cdot \mathbb{I}^{A}_{i,\phi,t} \leq T^{off}_{i,\phi,t} - T^{off}_{i,\phi,t-1} \leq 1 \tag{34}$$

$$T^{off}_{i,\phi,t} \geq DT_i \cdot (1 - \mathbb{I}^{on}_{i,\phi,t+1}) \tag{35}$$

$$\mathbb{I}^{on}_{i,\phi,t} + \mathbb{I}^{off}_{i,\phi,t} \leq 1 \tag{36}$$

$$\mathbb{I}^{on}_{i,\phi,t} - \mathbb{I}^{off}_{i,\phi,t} = \mathbb{I}^{A}_{i,\phi,t} - \mathbb{I}^{A}_{i,\phi,t-1} \tag{37}$$

The ammonia plant can be turned 'on' and 'off' at a rapid rate, on the order of minutes. Therefore, within an hour timeslot, the on and off time lags can be ignored in the model. Further, the ammonia plant is not able to instantaneously change its power consumption, but rather ramps up at $RU_i$ MW/h (38) and ramps down at $RD_i$ MW/h (39).

$$p^{D,A}_{i,\phi,t} - p^{D,A}_{i,\phi,t-1} \leq RU_i \tag{38}$$

$$p^{D,A}_{i,\phi,t-1} - p^{D,A}_{i,\phi,t} \leq RD_i \tag{39}$$

### 3.2. Fuel cell model

The power produced by the fuel cell ($p^{FC}_{i,\phi,t}$) is determined by the linear relationship between the amount of ammonia consumed by the fuel cell and the conversion rate, $p^{FC,R}$, as modeled

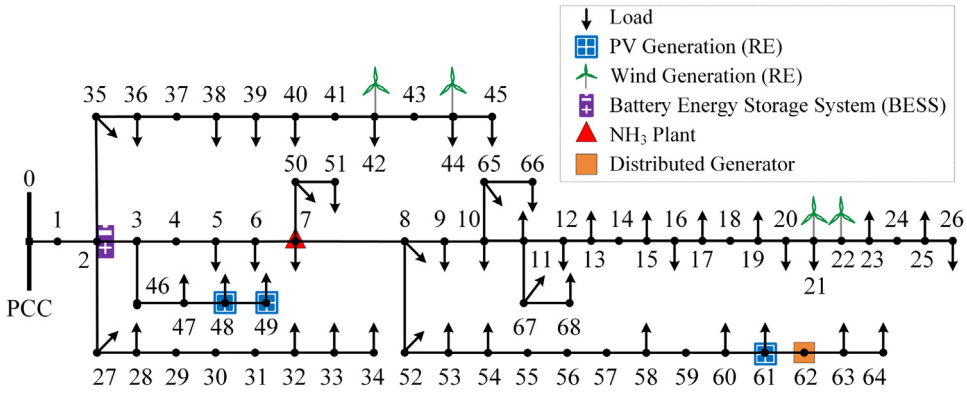


**Fig. 3.** An agricultural community microgrid based on a modified three-phase PG&E 69-node distribution system with diverse distributed energy resources coupled with an electricity-run ammonia production plant and a direct ammonia fuel cell.

in (40). The fuel cell is 'on' when the ammonia consumed by the fuel cell ($A^{FC}_{i,\phi,t}$) is between the minimum ($\underline{A^{FC}_{i,\phi,t}}$) and maximum ($\overline{A^{FC}_{i,\phi,t}}$) consumption rate of the fuel cell in tons, and is indicated by binary variable $\mathbb{I}^{FC}_{i,\phi,t}$ (41). The ammonia used by the fuel cell must be less than the amount of the on-site ammonia feedstock in the previous timeslot and the ammonia produced in that timeslot (42).

$$p^{FC}_{i,\phi,t} = p^{FC,R} \cdot A^{FC}_{i,\phi,t} \tag{40}$$

$$\underline{A^{FC}_{i,\phi,t}} \cdot \mathbb{I}^{FC}_{i,\phi,t} \leq A^{FC}_{i,\phi,t} \leq \overline{A^{FC}_{i,\phi,t}} \cdot \mathbb{I}^{FC}_{i,\phi,t} \tag{41}$$

$$\sum_{\phi} A^{FC}_{i,\phi,t} \leq A^{S}_{i,t-1} + A^{P}_{i,t} \tag{42}$$

### 3.3. Coupled system model

The coupled electricity and ammonia plant model is captured in the optimization problem $\mathbf{P_1}$. In this model, we consider the ammonia plant as a demand response system. The ammonia production is not optimized for the most profit, but all constraints, including the minimum required metric tons per day, must be met. Here, $p^{D}_{i,\phi,t}$ in (4) is a summation of the non-ammonia electrical demand and the optimized ammonia demand, $p^{D,A}_{i,\phi,t}$, associated with its respective node *i*. A similar coupling can be made for reactive power demand. The fuel cell real and reactive generation is included in the nodal power balance constraints (4) and (5). We define the coupled optimal power flow and ammonia production problem, $\mathbf{P_1}$, as:

$\mathbf{P_1}$: min(1)
subject to: (2)–(15), (24)–(42)

## 4. Case study

We consider a modified, unbalanced three-phase agricultural community microgrid based on the PG&E 69-node distribution system connected to a small-scale, electricity-run ammonia plant to validate our proposed model and investigate its impact on the DLMP. Fig. 3 shows a oneline diagram of the system. We consider a high renewable case with renewable generation units at Nodes 21, 22, 42, 44, 48, 49, and 61, with a maximum availability of 12.72 MW per phase. Three single-phase 0.5 MWh BESS units are on each phase at Node 2. The BESS was sized to aid in balancing the system. The unbalanced system, which follows a typical summer day load curve, sees a (non-ammonia) three-phase peak load of 14.55 MW. This is representative of a distribution feeder, which typically range from 0.6 to 28.5 MW per phase [57]. Further, a typical summer day is used, which exhibits the peak electrical load.

**Table 1**
Green ammonia plant parameters used in case study.

| | | | |
|---|---|---|---|
| $UT_i$ | 2 h | $DT_i$ | 6 h |
| $RU_i$ | 1 MW | $RD_i$ | 2 MW |
| $\underline{A^{S}_{i}}$ | 5 tons | $\overline{A^{S}_{i}}$ | 200 tons |
| $\underline{A^{P}}$ | 0.05 tons | $\overline{A^{P}}$ | 5 tons |
| $p^{D,AR}$ | 7.7 MWh/ton | $p^{D,W}$ | 0.002 MW |
| $\underline{A^{FC}_{i,\phi,t}}$ | 0.0025 ton/h | $\overline{A^{FC}_{i,\phi,t}}$ | 0.1 ton/h |
| $p^{FC,R}$ | 1.6 MWh/ton | | |

The balanced, three-phase energy demands of the green ammonia plant are included in the electrical demand for Node 7, and the fuel cell can independently provide power to each phase at Node 7. The substation LMP ranges from \$16.56/MWh to \$42.14/MWh, modeled after a typical summer day. A balanced, three-phase, 4.5 MW distributed generator is located at Node 62. This DG bids into the market at a cost higher than the LMP, \$61.69/MWh per phase, under the assumption that the marginal cost of a DG is more expensive than buying power from the grid. The historical data of Western Wind and Solar Integration Study [58] is modified and used for hourly samples of wind and PV generation.

The green ammonia plant, at minimum, must produce a desired 5 TPD of ammonia. Table 1 shows the green ammonia plant parameters considered in this study. The fuel cell is modeled after a futuristic, scaled-up direct ammonia fuel cell currently in the commercial market, the Gencell A5 fuel cell [59]. GAMS/CPLEX 28.1.0 [60] was used to solve the proposed MILP, $\mathbf{P_1}$. We define the following cases:

**Case 1 - Decoupled Electricity and Ammonia Models:** The ammonia plant operates without consideration of the grid conditions. The ammonia demand is fixed and must be met in the electricity model. The output of ammonia is exactly $\underline{A^{S}_{i}}$ tons. The electrical system is grid-connected and can buy and sell energy at the LMP of the substation node.

**Case 2 - Coupled Electricity and Ammonia Model:** The electric utility operates the ammonia plant, which acts as a demand-responsive system to best serve the electricity grid. The output of ammonia must be at least $\underline{A^{S}_{i}}$ tons but may exceed this value. The electrical system is grid-connected.

**Case 3 - Coupled Islanded Mode:** The agricultural microgrid is islanded. Buying and selling energy from the grid at the substation node is not allowed. The system must meet all

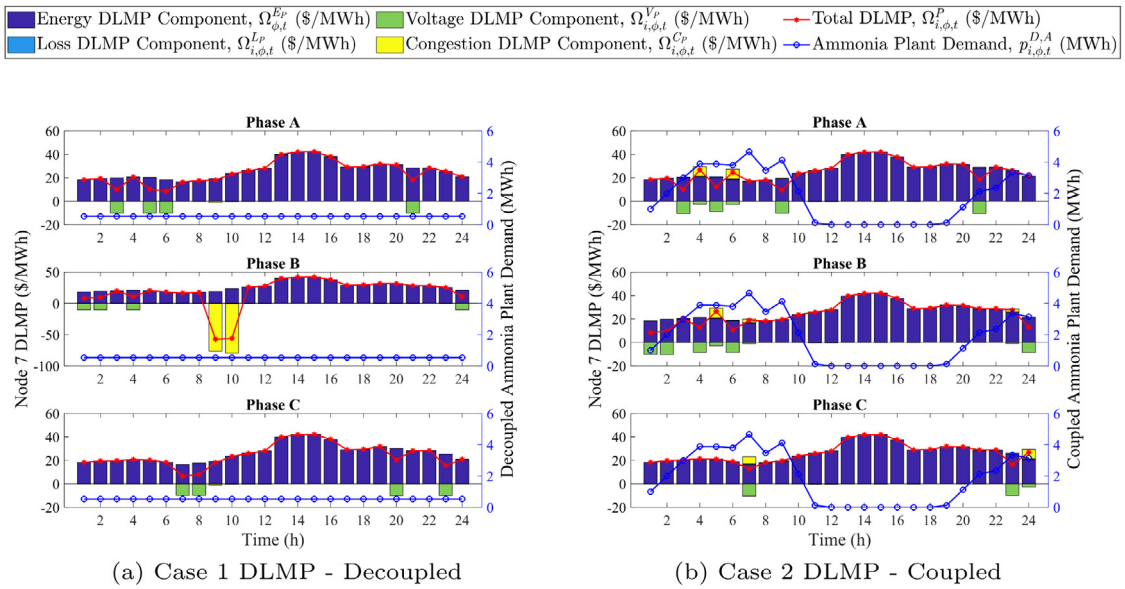


**Fig. 4.** Node 7 three-phase, component-wise DLMP comparison of decoupled and coupled models for the electricity distribution system and green ammonia plant (Cases 1 and 2). The flexible, green ammonia plant operates to ease operational burdens (voltage violation, line congestion) in the electric grid in the coupled case, improving the DLMP.

demands with the available DERs. The output of ammonia must be at least $\underline{A}^S_i$ tons but may exceed this value.

**Case 4 - Coupled Islanded Mode with Fuel Cell:** In this islanded agricultural microgrid, buying and selling energy from the substation node is not allowed. This case is an emergency situation where, perhaps, a natural disaster (e.g., hurricane) destroyed essential transmission lines that fed power to this system. Some of the distributed wind turbines must be shut down due to high wind speeds. The need for power outweighs the high cost of electricity. Therefore, the electric utility operates the typically high-cost fuel cell to best serve the islanded agricultural microgrid. The fuel cell operation has a cost associated with it, but at a relatively lower rate than the DG to discourage overuse of the fuel cell but allowing for liberal operation. The fuel used by the DG may have other uses during an emergency, so the cost associated with DG operation is higher than the fuel cell. In contrast, ammonia does not have other uses in a crisis.

The power demand is 30% of the normal demand. Wind speeds in the area are considered too high, and the wind turbines at buses 21, 22, 42, and 44 are shut down for safety purposes. Furthermore, a cloudy day is considered; therefore, the PV output is reduced and does not follow the typical sunny day curve. The desired TPD limit and 'on'/'off' constraints of the ammonia plant are relaxed in this emergency case. The initial stock of on-site ammonia for use by the fuel cell is 40 tons.

### 4.1. Impact on DLMP

The coupling of the green ammonia plant and the electrical system has a distinct impact on the three-phase DLMP, as shown in Fig. 4. Decoupled Case 1 considers the ammonia plant running at a constant load to produce the desired 5 tons by the end of the day. Case 1 sees many voltage violations and line congestion occurrences throughout the day, as shown with voltage and congestion DLMP components in Fig. 4(a), which are scaled-down to better understand the visualization. Further, power loss is unavoidable. Therefore, the system has loss DLMP components at every timeslot, though not all are visible due to their small size. Negative DLMP components indicate that the system would pay for extra load consumption to relieve operational issues. For example, many timeslots see negative voltage DLMP components due to the maximum voltage limit being met. The system would therefore benefit from more energy demand at that node to reduce the nodal voltage.

The decoupled green ammonia plant is unable to respond to the needs of the electrical system that are reflected in the DLMPs. Therefore, we consider a coupled green ammonia plant and electrical system in Case 2. The ammonia plant can serve as a demand-responsive load to the electricity distribution system and therefore improve the DLMP of the system by reducing voltage violations, line congestion, and RE curtailment to the best of the plant's ability. As shown in Fig. 4(b), the ammonia plant demand is higher when the DLMP is lower (indicating fewer issues in the electrical system) and lower when the DLMP is high. For example, the ammonia plant is in the 'warming' or 'off' state for Timeslots 12–18 in Case 2 due to the high DLMPs at this time.

Further, the coupled system completely removed the large, negative congestion DLMP components on Phase B in Timeslots 9 and 10 in the decoupled case. The ammonia plant consumes a balanced three-phase power, which must be considered when serving the electrical system. For example, Timeslot 4 sees congestion in the system on Phase A but a negative voltage component on Phase B. Considering the overall DLMP and all other constraints, the ammonia plant best serves the system by operating during this timeslot.

### 4.2. Impact of demand-responsive Green ammonia plant

In addition to the improvements on the DLMP mentioned previously, the coupled green ammonia plant also reduced the amount of RE curtailed in the system, as shown in Fig. 5. In all timeslots, the RE curtailment is lower in the coupled case. In Timeslots 8 and 20, the coupled system is able to completely remove the RE curtailment in the system by allowing the green ammonia plant to consume excess RE generation. The decoupled case requires a constant demand and increases the base, non-ammonia plant demand equally throughout the day. The coupled system increases the total demand in the system by storing excess RE in ammonia. In some timeslots, the renewable energy is completely utilized by the base demand. For example, the ammonia

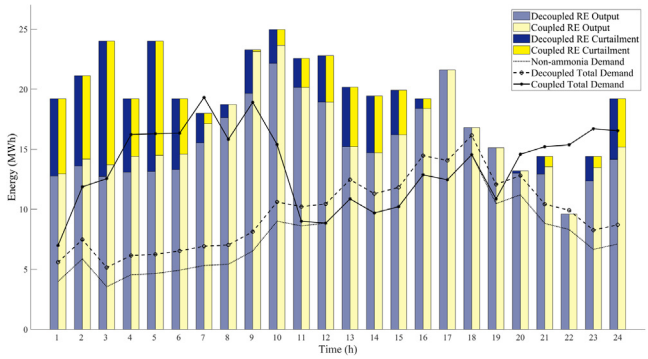


**Fig. 5.** Comparison of decoupled and coupled electrical system and green ammonia plant (Cases 1 and 2). Renewable energy curtailment reduces in the coupled case as the flexible demand from the green ammonia plant increases.

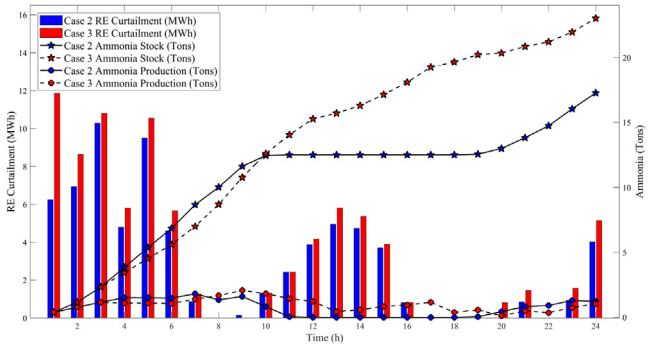


**Fig. 6.** Comparison of coupled grid-connected and islanded models (Cases 2 and 3). The curtailment increases in the islanded agricultural microgrid case as excess renewable energy cannot be sold to the grid. However, more ammonia is produced in Case 3 in attempt to reduce this curtailment. (For interpretation of the references to color in this figure legend, the reader is referred to the web version of this article.)

plant is 'warming' in Timeslots 12–16 and 'off' in Timeslots 17–18 to not increase the load further and require more expensive energy from the substation node or the distributed generator as the total energy cost is minimized in the objective function. The green ammonia plant operates in a manner that attempts to level out the demand throughout the day.

Notice in most timeslots, the RE is still curtailed even in the coupled case. Nodal voltage limits being met and or congested lines in the system cause the RE curtailment, which is graphically depicted in Fig. 4(b). This curtailment indicates the importance of smart DER planning and grid upgrades to handle large amounts of distributed renewable energy resources expected in future distribution systems. Further, in both cases, the renewable energy is sold to the substation node at LMP until a constraint is met and it can no longer sell the excess energy. The flexible demand from the ammonia plant allows some of the curtailed RE in the previous case to be consumed by the ammonia plant. Due to the incentive in the objective function for selling excess energy, the system will attempt this option first and then store excess RE as ammonia. Therefore, we next consider an islanded system to compare the impact of the green ammonia plant on the system when there is no option to sell excess renewable energy to the larger grid.

The comparison between coupled grid-connected and islanded models is depicted in Fig. 6. As expected, the renewable energy curtailment is greater in the case of the islanded model (shown in red) in all timeslots except 9, as the excess RE cannot be exported to the grid. A voltage limit is met in Timeslot 9 on Node 22 that forces the curtailment in Case 2. The green ammonia plant consumes as much of the excess RE in the islanded case that the constraints for both the ammonia plant and the agricultural microgrid allow, and the rest is curtailed at a penalty. Therefore, we see a larger stock of ammonia at the end of the day in the islanded case, Case 3. In Case 2 (shown in blue), the hourly ammonia production is zero for Timeslots 12–18. The system would rather sell as much excess RE as the system allows than produce excess green ammonia. The ammonia produced and the utilization of the renewable energy in the system for each case are outlined in Table 2. Case 2 shows an improvement in renewable energy utilization over Case 1 while producing over three times the amount of ammonia by the end of the day. The RE utilization decreases in Case 3 as the system is islanded, and excess RE can no longer be sold back to the grid. However, more ammonia is produced by the end of the day to maximize the amount of RE used in the system. Under the emergency scenario in Case 4, the total available renewable energy was utilized while producing ammonia only in timeslots with excess RE. Case 4 will be further discussed in the following section.

**Table 2**
Case study results comparison.

| | Case 1 | Case 2 | Case 3 | Case 4 |
|---|---|---|---|---|
| Tons of Ammonia | 5 | 17.27 | 23.00 | 0.72 |
| RE utilization | 81.02% | 84.56% | 81.01% | 100% |

To investigate the financial impact of this coupling, simplified ammonia plant electricity costs and profits are calculated post-solve. The real and reactive DLMPs at Node 7 are multiplied to the ammonia plant electricity demand in Cases 1 and 2 to calculate the true electricity costs of the ammonia plant. Electricity costs of $869.36 and $2665.66 were computed for Cases 1 and 2, respectively. Recall the ammonia produced in Case 1 is 5.00 tons, and the amount produced in Case 2 is 17.27 tons. Ammonia prices are historically quite variable, with prices soaring over $1000 per ton in 2021 [61]. However, the minimum average selling price of ammonia in years 2008–2014 was $499 per ton of ammonia [62]. Therefore, this conservative market value is used to find the simplified profit (only considering electricity costs) from selling ammonia. The daily profits calculated for Case 1 and Case 2 are, respectively, $1625.64 and $5952.71.

A decoupled case producing 17.27 tons of ammonia per day and a coupled case producing 5.00 TPD are studied for a better comparison. However, the decoupled case is designed to use a constant power consumption across all timeslots by the ammonia plant. The total electricity cost of this case is $3512.13, nearly a 32% increase in the coupled case's (Case 2) electricity cost. This higher cost results in the coupled case's daily profit exceeding that of the decoupled case by more than 16%. Next, a coupled case held to 5.00 TPD is compared to Case 1. The flexible plant produced ammonia when DLMPs were low. Electricity costs drop by nearly a third, with the electricity cost of the ammonia plant being $590.64. Ammonia plant daily profits increase 17% in this case. The ammonia plant financially benefits from the flexible coordination with the electricity DSO. Table 3 summarizes the results of this analysis.

### 4.3. Impact of ammonia fuel cell in emergency state

The total system energy in Case 4 for each timeslot is depicted in Fig. 7. The renewable energy exceeds the base, non-ammonia plant demand in Timeslots 8 and 11–16. Under the assumption that all critical loads are met, excess RE can be consumed by the ammonia plant and made available for future energy use through the fuel cell. Due to the duration of the outage being unknown,

**Table 3**
Daily economic performance for alternative configurations of ammonia production.

| Configuration | Tons $NH_3$ | Ammonia revenue | Electricity cost | Ammonia profit |
|---|---|---|---|---|
| Coupled | 5.00 | $2495.00 | $590.64 | $1904.36 |
| Decoupled (Case 1) | 5.00 | $2495.00 | $869.36 | $1625.64 |
| Coupled (Case 2) | 17.27 | $8618.38 | $2665.66 | $5952.71 |
| Decoupled | 17.27 | $8618.38 | $3512.13 | $5106.24 |

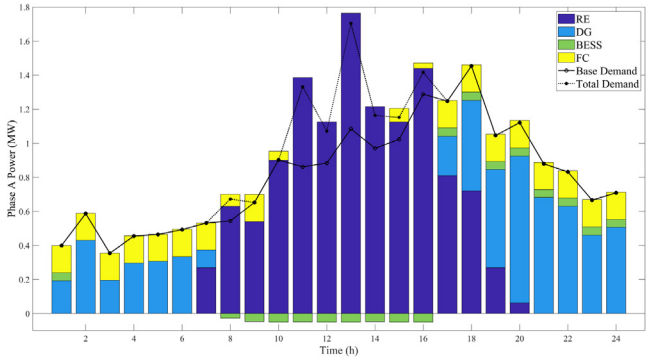


**Fig. 7.** Phase A total power generation and demand in an emergency state (Case 4). The flexible green ammonia plant operates when the RE generation goes beyond the critical demand. The fuel cell operates to provide essential power to the weakened agricultural microgrid.

energy storage is recommended during this time so valuable energy is not wasted. In all other timeslots, the renewable energy in the system is not enough to meet the base demand. Therefore, the system relies on the BESS, direct ammonia fuel cell, and the distributed generator. The battery does not bid into the system and is used freely to best serve the system. Thus, the BESS charges during times of high RE and discharges at timeslots later in the day that do not have RE available. The fuel cell bids at a lower cost than the DG, and the system utilizes this resource in many timeslots. The fuel cell alone is not enough in most cases, as it has a relatively small power output. Therefore, the high-cost DG operates to make up for the necessary generation.

Note, in most cases, the green ammonia itself is the value-added commodity. In the case of an emergency, when the price of electricity is extremely high, converting the green ammonia back to electrons may be more cost-effective than selling to the bulk ammonia market. In an emergency, supplying power to the most critical loads (e.g., life-supporting loads) is more important than the cost of electricity.

## 5. Conclusion

The case studies provide numerical evidence that indicate the advantages of using a green ammonia plant as a flexible load and storage solution for agricultural community microgrids. The following observations are made for the first time.

- The DLMP can be favorably impacted by coupling the flexible green ammonia plant to the agricultural microgrid. Congestion and or voltage violations can be reduced or removed by optimally scheduling the ammonia plant with respect to grid conditions. Operational challenges in the microgrid with high levels of RE can be mitigated as a result of this coordination.
- The flexible operation of the green ammonia plant reduces the curtailment of renewable energy sources in a high penetration scenario. This is achieved by creating additional ammonia to consume excess renewable generation.
- By optimally controlling the green ammonia plant, the electricity demand shifts away from the peak electricity time to times with greater available renewable energy. A benefit of the coordination between the microgrid and the ammonia plant is the ability to shift demands to times where renewable energy would have otherwise been curtailed in a high renewable energy scenario. Also, reducing peak demands by allowing the ammonia plant to consume minimal energy in the 'warming' mode provides additional relief to the microgrid.
- As a result of this coupling, ammonia plant economics can be improved. Case studies showed electricity costs of the coupled ammonia plant could be reduced due to the plant operating in timeslots with lower DLMPs. Therefore, ammonia plants can gain higher profits when coupled with the optimal operation of the electricity grid.
- Through the chemical energy storage capabilities of ammonia, the coordinated agricultural microgrid and green ammonia plant offer a unique solution for storing excess renewable energy. The excess renewable energy will be stored in ammonia and sold to the bulk ammonia or hydrogen market or used as electricity through the direct ammonia fuel cell. An advantage of chemical energy storage in ammonia over traditional batteries is long-term storage capability.
- The fuel cell offers additional power generation to the agricultural microgrid in emergencies or when the price of electricity is very high. Otherwise, green ammonia is more profitable when sold to the bulk ammonia or hydrogen market. The fuel cell allows this form of energy storage to be sold back to the grid, similar to a traditional battery but at a lower round-trip efficiency. The ability to sell ammonia directly differentiates this storage solution from a traditional battery.

A novel coordinated electricity and green ammonia plant model was formulated and validated on an agricultural community microgrid based on the PG&E 69-node distribution system. The impact of coupling the electrical system and the green ammonia plant on the DLMP was shown for the first time. This cooperation could strengthen future electricity distribution markets that consider DLMP. Further, the proposed model and method can offer utilities a unique tool in managing high renewable energy scenarios by coupling electricity distribution systems and green ammonia plants for storage and demand response solutions.

Not studied in this work is the cost of electricity incurred to the ammonia plant by storing excess renewable energy in ammonia. Quantifying a financial incentive for demand response services beyond the benefits of DLMP is interesting future work and can be easily added to the proposed model. Further, this work may impact policies regarding agricultural community microgrids with significant amounts of renewable energy resources.

To enhance the impact of the demand-responsive green ammonia plant, the anhydrous ammonia fuel and the direct ammonia fuel cell can be moved to other locations (nodes) in the system in the case of voltage instability, thermal line limits being met, or an emergency. Therefore, mobile fuel cells allow not only the temporal storage of electricity but also locational storage. The power generated by the fuel cell could serve any node in need and is not limited to a single node as most stationary power

generators are. The total cost of this, including fuel and fuel cell transport, would have to be less than the elevated DLMP at this location.

This study can be adapted to analyze a variety of flexible loads with storage capabilities, each with unique considerations of advantages, drawbacks, and constraints. Our future work includes the consideration of the variability of renewable energy generation using stochastic programming techniques and the development of a dynamic decision-making tool to assist with smart planning of the proposed technology and method.

## CRediT authorship contribution statement

**Lawryn Edmonds:** Methodology, Software, Investigation, Writing – original draft. **Peter Pfromm:** Validation, Resources, Writing – review & editing, Supervision. **Vincent Amanor-Boadu:** Supervision. **Mary Hill:** Writing – review & editing, Supervision, Funding acquisition. **Hongyu Wu:** Conceptualization, Supervision, Project administration.

## Declaration of competing interest

The authors declare that they have no known competing financial interests or personal relationships that could have appeared to influence the work reported in this paper.

## Acknowledgments

This work was supported by the National Science Foundation, United States Grant 1856084 for the FEWtures project.

## References

[1] R.J. Bravo, R. Salas, T. Bialek, C. Sun, Distributed energy resources challenges for utilities, in: 2015 IEEE 42nd Photovoltaic Specialist Conference (PVSC), 2015, pp. 1–5.
[2] R. Bessa, C. Moreira, B. Silva, M. Matos, Handling renewable energy variability and uncertainty in power systems operation, WIREs Energy Environ. 3 (2) (2014) 156–178.
[3] T. Edmunds, et al., The Value of Energy Storage and Demand Response for Renewable Integration in California, California Energy Commission, 2017, p. 241.
[4] P.J. Heptonstall, R.J.K. Gross, A systematic review of the costs and impacts of integrating variable renewables into power grids, Nat. Energy 6 (1) (2021) 1.
[5] P. Denholm, Y.H. Wan, M. Hummon, M. Mehos, Analysis of Concentrating Solar Power with Thermal Energy Storage in a California 33% Renewable Scenario, Tech. Rep. NREL/TP-6A20-58186, Nat. Renewable Energy Lab., Golden, CO, USA, 2013, 1072790.
[6] A. Botterud, T. Levin, V. Koritarov, Pumped Storage Hydropower: Benefits for Grid Reliability and Integration of Variable Renewable Energy, Report ANL/DIS-14/10, Argonne Nat. Lab., 2014.
[7] E. Ela, Role of Pumped Storage Hydro Resources in Electricity Markets and System Operation: Preprint, NREL Conference Paper, 2013, p. 12.
[8] Community microgrids, 2021, Clean Coalition. https://clean-coalition.org/community-microgrids/ (accessed Oct. 16, 2021).
[9] Ameren Services Company, Complainants' Brief of Ameren Services Company and Northern Indiana Public Service Company, Docket Nos. EL07-86-000, EL07-88-000, EL07-92-000, Federal Energy Regulatory Commission, 2008, p. 2.
[10] W.M. Stewart, D.W. Dibb, A.E. Johnston, T.J. Smyth, The contribution of commercial fertilizer nutrients to food production, Agron. J. 97 (2005) 1–6.
[11] J.N. Galloway, et al., Transformation of the nitrogen cycle: Recent trends, questions, and potential solutions, Science 320 (5878) (2008) 889–892.
[12] A. Valera-Medina, H. Xiao, M. Owen-Jones, W.I.F. David, P.J. Bowen, Ammonia for power, Prog. Energy Combust. Sci. 69 (2018) 63–102.
[13] S. Giddey, S.P.S. Badwal, C. Munnings, M. Dolan, Ammonia as a renewable energy transportation media, ACS Sustain. Chem. Eng. 5 (11) (2017) 10231–10239.
[14] T. Lipman, N. Shah, Ammonia As an Alternative Energy Storage Medium for Hydrogen Fuel Cells, Final Report Caltrans/UC Berkeley Contract #22A0418, Task Order 1, U.C. Berkeley Transportation Sustainability Research Center, 2007.
[15] J.S. Cardoso, V. Silva, R.C. Rocha, M.J. Hall, M. Costa, D. Eusébio, Ammonia as an energy vector: Current and future prospects for low-carbon fuel applications in internal combustion engines, J. Cleaner Prod. 296 (2021) 126562.
[16] N. Salmon, R. Bañares-Alcántara, Green ammonia as a spatial energy vector: a review, Sustain. Energy Fuels 5 (11) (2021) 2814–2839.
[17] P. Pfromm, Towards sustainable agriculture: fossil-free ammonia, J. Renew. Sustain. Energy 9 (3) (2017).
[18] M. Dubey, F. Young, R. Hlavin, K. Johnson, Conversion and storage of wind energy as nitrogenous fertilizer, in: 12th Intersociety Energy Conversion Engineering Conference, Vol. 1, 1977, pp. 525–532.
[19] L. Bassett, et al., Revolution…now the Future Arrives for Five Clean Energy Technologies–2015 Update, United States Department of Energy, 2015, p. 24.
[20] P. Han, H. Topsoe, Dynamic Green Ammonia By Haldor Topsoe, NK2 Workshop, 2021.
[21] W. Huang, Impact of Rising Natural Gas Prices on U.S. Ammonia Supply, A Report from the Economic Research Service USDA, 2007, p. 19.
[22] Natural gas futures contract 1 (dollars per million btu), 2021, https://www.eia.gov/dnav/ng/hist/rngc1A.htm (accessed Oct. 16, 2021).
[23] Average energy prices for the United States, regions, census divisions, and selected metropolitan areas: Midwest information office: U.S. Bureau of Labor Statistics, 2021, https://www.bls.gov/regions/midwest/data/averageenergyprices_selectedareas_table.htm (accessed Oct. 18, 2021).
[24] C. Zhang, et al., Flexible grid-based electrolysis hydrogen production for fuel cell vehicles reduces costs and greenhouse gas emissions, Appl. Energy 278 (2020) 115651.
[25] O. Elishav, et al., Progress and prospective of nitrogen-based alternative fuels, Chem. Rev. 120 (12) (2020) 5352–5436.
[26] K.H.R. Rouwenhorst, A.G.J. Van der Ham, G. Mul, S.R.A. Kersten, Islanded ammonia power systems: Technology review & conceptual process design, Renew. Sustain. Energy Rev. 114 (2019) 109339.
[27] P. Capros, N. Tasios, A. Marinakis, Very high penetration of renewable energy sources to the European electricity system in the context of model-based analysis of an energy roadmap towards a low carbon EU economy by 2050, in: 2012 9th International Conference on the European Energy Market, 2012, pp. 1–8.
[28] A. Valera-Medina, R. Banares-Alcantara, Techno-Economic Challenges of Green Ammonia As an Energy Vector, Academic Press, 2020.
[29] B. Lin, T. Wiesner, M. Malmali, Performance of a small-scale haber process: A techno-economic analysis, ACS Sustain. Chem. Eng. 8 (41) (2020) 15517–15531.
[30] M. Wang, et al., Can sustainable ammonia synthesis pathways compete with fossil-fuel based Haber–Bosch processes? Energy Environ. Sci. 14 (5) (2021) 2535–2548.
[31] M. Fasihi, R. Weiss, J. Savolainen, C. Breyer, Global potential of green ammonia based on hybrid PV-wind power plants, Appl. Energy 294 (2021) 116170.
[32] J. Ikäheimo, J. Kiviluoma, R. Weiss, H. Holttinen, Power-to-ammonia in future north European 100% renewable power and heat system, Int. J. Hydrogen Energy 43 (36) (2018) 17295–17308.
[33] R. Nayak-Luke, R. Bañares-Alcántara, I. Wilkinson, 'Green' ammonia: Impact of renewable energy intermittency on plant sizing and levelized cost of ammonia, Ind. Eng. Chem. Res. 57 (43) (2018) 14607–14616.
[34] Z. Cesaro, M. Ives, R. Nayak-Luke, M. Mason, R. Bañares-Alcántara, Ammonia to power: Forecasting the levelized cost of electricity from green ammonia in large-scale power plants, Appl. Energy 282 (2021) 116009.
[35] L. Wang, et al., Greening ammonia toward the solar ammonia refinery, Joule 2 (6) (2018) 1055–1074.
[36] J. Li, et al., Co-planning of regional wind resources-based ammonia industry and the electric network: A case study of inner mongolia, IEEE Trans. Power Syst. (2021).
[37] E.F. Bødal, D. Mallapragada, A. Botterud, Decarbonization synergies from joint planning of electricity and hydrogen production: A texas case study, Int. J. Hydrogen Energy 45 (2020) 32899–32915.
[38] L. Edmonds, M. Derby, M. Hill, H. Wu, Coordinated operation of water and electricity distribution networks with variable renewable energy and distribution locational marginal pricing, Renew. Energy 177 (2021) 1438–1450.
[39] Z. Yang, C. Gao, M. Zhao, Coordination of integrated natural gas and electrical systems in day-ahead scheduling considering a novel flexible energy-use mechanism, Energy Convers. Manage. 196 (2019) 117–126.
[40] E.F. Bødal, M. Korpås, Value of hydro power flexibility for hydrogen production in constrained transmission grids, Int. J. Hydrogen Energy 45 (2020) 1255–1266.
[41] A. Hajimiragha, M.W. Fowler, C.A. Cañizares, Hydrogen economy transition in ontario – Canada considering the electricity grid constraints, Int. J. Hydrogen Energy 34 (13) (2009) 5275–5293.

[42] F. vom Scheidt, J. Qu, P. Staudt, D.S. Mallapragada, C. Weinhardt, Integrating hydrogen in single-price electricity systems: The effects of spatial economic signals, Energy Policy 161 (2022) 112727.
[43] D. Xu, et al., Integrated modelling and enhanced utilization of power-to-ammonia for high renewable penetrated multi-energy systems, IEEE Trans. Power Syst. 35 (6) (2020) 4769–4780.
[44] O. Siddiqui, I. Dincer, Development and evaluation of a solar-based integrated ammonia synthesis and fuel cell system, J. Cleaner Prod. 256 (2020) 120393.
[45] A. Allman, P. Daoutidis, Optimal scheduling for wind-powered ammonia generation: Effects of key design parameters, Chem. Eng. Res. Des. 131 (2017) 5–15.
[46] S.S. Beerbühl, M. Fröhling, F. Schultmann, Combined scheduling and capacity planning of electricity-based ammonia production to integrate renewable energies, European J. Oper. Res. 241 (3) (2015) 851–862.
[47] K. Rouwenhorst, L. van der Ham, G. Mul, S. Kersten, Power-to-ammonia-to-power (P2A2P) for local electricity storage in 2025, in: 15th Annual NH3 Fuel Conference, Pittsburgh, PA, 2018.
[48] M. Shahidehpour, H. Wu, Hourly demand response as an alternative to flexible ramping of thermal units in stochastic operation of electric power systems with non-dispatchable energy sources, in: Handbook of Clean Energy Systems, 2015.
[49] E. Ela, et al., Future electricity markets: Designing for massive amounts of zero-variable-cost renewable resources, IEEE Power Energy Mag. 17 (6) (2019) 58–66.
[50] L. Edmonds, M.N. Faqiry, H. Wu, A. Palani, Three-phase distribution locational marginal pricing to manage unbalanced variable renewable energy, in: 2020 IEEE Power & Energy Society General Meeting (PESGM), 2020.
[51] M.N. Faqiry, L. Edmonds, H. Zhang, A. Khodaei, H. Wu, Transactive-market-based operation of distributed electrical energy storage with grid constraints, Energies 10 (11) (2017) 1891.
[52] M.N. Faqiry, L. Edmonds, H. Wu, A. Pahwa, Distribution locational marginal price-based transactive day-ahead market with variable renewable generation, Appl. Energy 259 (2020) 114103.
[53] H. Yuan, F. Li, Y. Wei, J. Zhu, Novel linearized power flow and linearized OPF models for active distribution networks with application in distribution LMP, IEEE Trans. Smart Grid 9 (1) (2018) 438–448.
[54] J.A. Taylor, Convex Optimization of Power Systems, Cambridge University Press, 2015.
[55] M. İnci, Active/reactive energy control scheme for grid-connected fuel cell system with local inductive loads, Energy 197 (2020) 117191.
[56] M.Y. El-Sharkh, A. Rahman, M.S. Alam, A.A. Sakla, P.C. Byrne, T. Thomas, Analysis of active and reactive power control of a stand-alone PEM fuel cell power plant, IEEE Trans. Power Syst. 19 (4) (2004) 2022–2028.
[57] M.J. Reno, R.J. Broderick, Statistical analysis of feeder and locational PV hosting capacity for 216 feeders, in: IEEE Power and Energy Society General Meeting (PESGM), 2016.
[58] D. Lew, et al., The Western Wind and Solar Integration Study Phase 2, Vol. 1220243, Tech. Rep. NREL/TPe5500-55588, Nat. Renewable Energy Lab., Golden, CO, USA, 2013.
[59] A5$^{TM}$ off grid power solution | GenCell, GenCell - fuel cell generators, 2021, https://www.gencellenergy.com/our-products/gencell-a5/ (accessed Apr. 05, 2021).
[60] GAMS Development Corporation, General Algebraic Modeling System (GAMS) Release 28.1.0, GAMS Development Corporation, Washington, DC, USA, 2019.
[61] J. Outlaw, B. Fischer, H. Bryant, J.M. Raulston, Economic Impact of Nitrogen Prices on U.S. Corn Producers, Texas A & M Agricultural and Food Policy Center, 2021.
[62] R. Mosheim, Fertilizer Use and Price, USDA Economic Research Service, Department of Agriculture, 2019, Accessed on: Feb. 16, 2022. [Online]. Available: https://data.nal.usda.gov/dataset/fertilizer-use-and-price.